PROCEEDINGS OF SCIENCE

Offline calibrations and performance of the ATLAS Pixel Detector

A. Andreazza*, **on behalf of the ATLAS Collaboration**
INFN Sezione di Milano and Dipartimento di Fisica, Università di Milano, Via Celoria 16, I-20133, Milano, Italy
E-mail: Attilio.Andreazza@mi.infn.it

The ATLAS Pixel Detector is the innermost detector of the ATLAS experiment at the Large Hadron Collider at CERN. It consists of 1744 silicon sensors equipped with approximately 80 millions electronic channels, providing typically three measurement points with high resolution for charged particles emerging from the beam-interaction region, thus allowing the measurement of particle tracks and secondary vertices with very high precision. In this talk the performance reached by the Pixel Detector with LHC collision data is presented, with particular attention to its spatial resolution, efficiency, particle identification properties and the measurement of the Lorentz angle. Examples of applications of the Pixel Detector performance in physics results are also shown.

10th International Conference on Large Scale Applications and Radiation Hardness of Semiconductor Detectors,
July 6-8, 2011
Firenze Italy

*Speaker.

PoS(RD11)006

1. Introduction

ATLAS [1] is a general purpose particle physics experiment at the Large Hadron Collider at CERN. The Pixel Detector [2] is the innermost component of its tracking system and consists of hybrid silicon pixels.

The Pixel Detector started operation in 2008 with cosmic-ray data-taking [3] and its operational experience with proton-proton collisions is described in [4]. To fully exploit the detector performance, offline calibration procedures are implemented. They consist in monitoring the noise and efficiency, in calibrating the charge sharing algorithm for the determination of the particle crossing-points and in measuring the Lorentz angle and the specific energy loss. After a brief description of the detector structure the performance in terms of efficiency and resolution are described together with the relevant calibration procedures in Sections 3 and 4. Lorentz angle and specific energy loss measurements will be summarized in Sections 5 and 6, respectively. Overall tracking performance is discussed in [5], but some specific applications of the assessed detector performance are provided in the relevant sections.

2. The ATLAS Pixel Detector

The ATLAS Pixel Detector is made of three barrel layers (with radii 50.5 mm, 88.5 mm and 122.5 mm and 800 mm length) and two end-caps, each one constituted of three disks (located at 495 mm, 580 mm and 650 mm from the detector centre). It provides three precision measurement points for tracks with pseudorapidity $|\eta| < 2.5$. The detector layout is shown in Fig. 1.

The basic components of the detector are the modules, that are identical for barrel layers and disks. In the barrel they are arranged in overlapping staves of 13 modules each, while in the disks they form 6-module sectors, for a total of 1744 modules. Each module consists of a n^+-in-n silicon sensor, segmented in a 324 rows and 144 columns matrix of pixels, 16 front-end chips and a flex hybrid containing control and transmission electronics [2]. The typical pixel size is 50×400 μm^2. The total amounts to more than 80×10^6 pixels covering a surface of 1.7 m^2.

The 50 μm pixel edge is oriented perpendicularly to the 2 T magnetic field generated by the ATLAS solenoid and defines the local-x coordinate, while the local-y coordinate is oriented along the 400 μm pixel edge and the local-z coordinate is perpendicular to the sensor surface.

All components are designed to sustain the radiation dose of 500 kGy, which is expected during the detector lifetime. The detector structure is made of low-mass carbon fibres and integrates the cooling system, resulting in a total contribution to the radiation length of about 3% per layer.

3. Efficiency

The intrinsic efficiency of the detector before radiation damage has been measured to be greater than 99.9% both in test-beam data [6] and with cosmic-ray muons [3]. The detector efficiency is therefore dominated by inactive regions: non-operational modules, defective front-end chips and noisy or defective pixels.

Currently the number of non-operational modules is 55 (3.2%), and there are 47 defective front-end chips, corresponding to an additional inefficiency of 0.16%. Offline the detection of

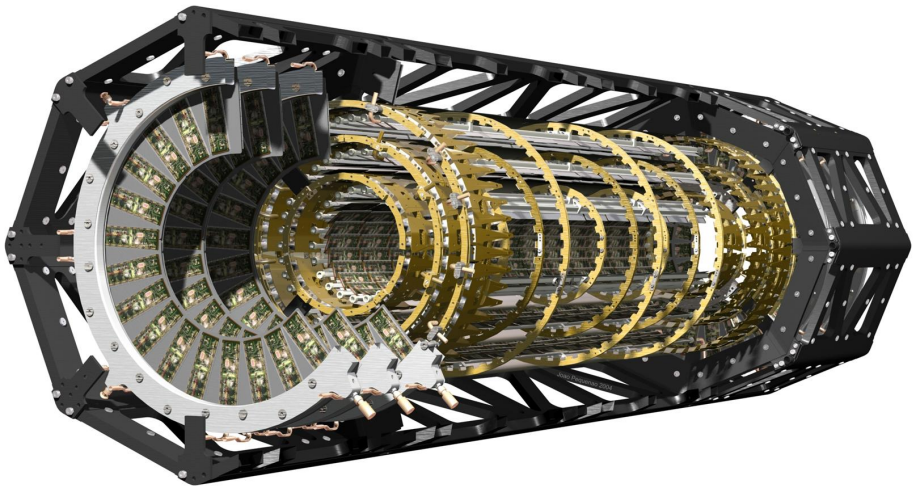

Figure 1: Computer generated image of the ATLAS Pixel Detector.

these defects is performed on two special data streams which are both acquired at a 10 Hz rate during data-taking: random triggers when beams are not present in the detectors are used to tag noisy pixels, and a mixture of physics triggers, dubbed *express stream*, is used to monitor non-operational channels. Noise maps are produced approximately for every LHC fill and masking few thousands pixels with noise occupancy greater than 10^{-5} results in a noise occupancy better than 10^{-9} as shown in Fig. 2, in agreement with the expectations from the analysis of cosmic-ray data [3]. Due to the low pixel occupancy, maps of non-operational channels are compiled only after integrating several millions of events in the *express stream*. Approximately 260000 pixels out of 80 millions are found defective, half of them due to the above mentioned defective front-end chips and most of the others due to few modules with damaged bump-bonds. An example is given on the right side of Fig. 2. These damages were found during the detector construction and have been stable during the LHC operation to date.

The precision estimation of track reconstruction efficiency and quality relies on a good description of these inefficiencies. This is particularly challenging in high-occupancy events, like the heavy-ion collisions [7]. The excellent agreement between the simulation and data collected in the 2010 Pb-Pb collisions at the nucleon-nucleon centre of mass energy $\sqrt{s_{\mathrm{NN}}} = 2.76$ TeV (Fig. 3 left) is obtained by feeding the simulation with the detailed inefficiency maps derived in the offline calibration procedure. The measurement of charged particle yields was performed using pixel-only tracks [8]. The right side of Fig. 3 shows the results of three different methods: the *pixel tracks* method considers tracks consisting of three pixel points, *method 1* and *method 2* use tracks built from the collision vertex and two pixel points. The difference between the latter two methods is that *method 1* performs a combinatorial subtraction based on simulation, while *method 2* uses a data-driven approach [8]. The three methods largely differ in acceptance and combinatorial background, but agree within 5% after the Monte Carlo based efficiency corrections.

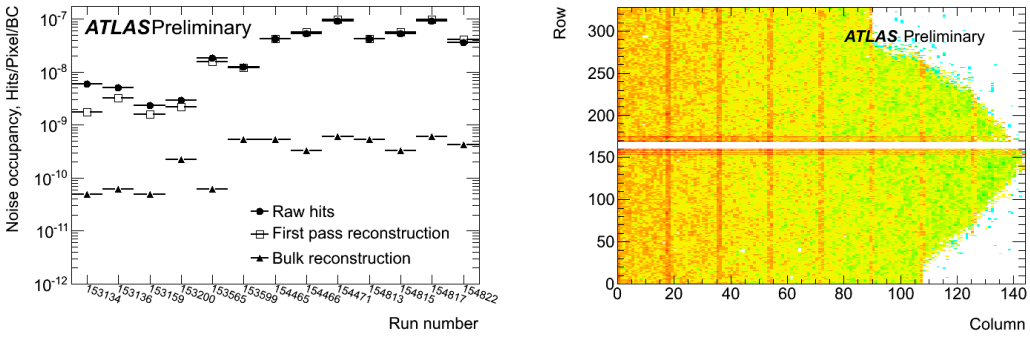

Figure 2: Left panel: noise occupancy in the Pixel Detector (left) before noise suppression (raw hits), after applying a static noise mask (first pass reconstruction) and after the offline calibration (bulk reconstruction). Right panel: hit-map of the module with the highest number of damaged bump-bonds. The empty horizontal line corresponds to pixels in the gap between the two rows of front-end chips. These pixels are ganged to nearby channels (visible as higher occupancy horizontal lines) [2].

4. Spatial resolution

The spatial resolution depends on the readout tuning, on the cluster size and on the particle incident angle. It is improved by adding to the geometrical centre of a cluster of pixels, whose coordinates (x_c, y_c) are defined respectively as the midpoint of the first and last rows and columns of the cluster, a correction term dependent on the sharing of the collected signal among the individual pixels in the cluster. The *charge sharing* variables, Ω_x and Ω_y, are defined as the ratio between the charge collected respectively in the last row (last column) of the cluster and the sum of charges collected in both the first and last rows (columns):

$$\Omega_x = \frac{Q_{\text{last row}}}{Q_{\text{first row}} + Q_{\text{last row}}} \qquad \Omega_y = \frac{Q_{\text{last column}}}{Q_{\text{first column}} + Q_{\text{last column}}} \tag{4.1}$$

The weights Δ_x and Δ_y for the correction

$$(x_c, y_c) \rightarrow (x_c + \Delta_x \cdot (\Omega_x - 1/2), y_c + \Delta_y \cdot (\Omega_y - 1/2)) \tag{4.2}$$

are obtained from data, from the linear dependence of the distance between the extrapolated track and the cluster center on the $\Omega_{x(y)}$ variables. They are computed for different cluster sizes and ranges of the incident angle [9]. The improvement in resolution after the calibration of the *charge sharing* correction is shown in Fig. 4 by evaluating the R.M.S. of the residuals between the track extrapolation and the measured position. Notice the width of the residuals is significantly bigger than the intrinsic detector resolution [10], which is a factor 2–3 better, because of the contribution from the track extrapolation uncertainty.

The contribution of the excellent pixel resolution to the ATLAS tracking performance is described in [5]. As an example, the accuracy in the reconstruction of the vertexes due to hadronic interactions in the Pixel Detector allows for an accurate mapping of the detector material, as illustrated in Fig. 5 [11]. The cooling pipe, connectors and cables are visible at positive local-z, the rectangle at local-$x \approx -5$ mm and local-$z \approx -2$ mm and the smaller one at local-$x \approx -8$ mm and local-$z \approx -1$ mm are due to passive components on the flex-hybrid.

5. Lorentz angle

The ATLAS detector uses a 2 T solenoidal magnetic field to measure the momentum of charged particles in the inner tracker. The field causes charge carriers inside the Pixel Detector sensor to drift towards the electrodes forming an angle with respect to the electric field, normal to the module surface, the *Lorentz angle* θ_{L}. When reconstructing the particle crossing point, the shift of the collected charge due to the change in drift direction amounts to $\approx 30\ \mu$m and needs to be corrected [10]. The distribution of the cluster size as a function of the particle incident angle is used to measure an effective Lorentz angle, which corresponds to the minimum of this distribution. The average cluster size, projected on the local-x direction ranges from 1.4 at its minimum up 2.6 for particle at high incident angle. A full study of the systematic uncertainties was performed on cosmic-ray data [3], giving a value of $\theta_{\mathrm{L}} = 11.77^\circ \pm 0.03^\circ \pm^{0.13^\circ}_{0.23^\circ}$ at -3°C and a temperature dependence of $\mathrm{d}\theta_{\mathrm{L}}/\mathrm{d}T = (-0.042 \pm 0.003)^\circ/\mathrm{K}$ (Fig. 6 left). With collision data, both at centre-of-mass energies of 900 GeV and 7 TeV, the measurement is less accurate, due to the smaller range of particle incident angles (Fig. 6 right). The mean temperature of the detector is lower, resulting in a larger θ_{L}. The measured value of $12.1^\circ \pm 0.09^\circ$ agrees with the expectations of the model in [10].

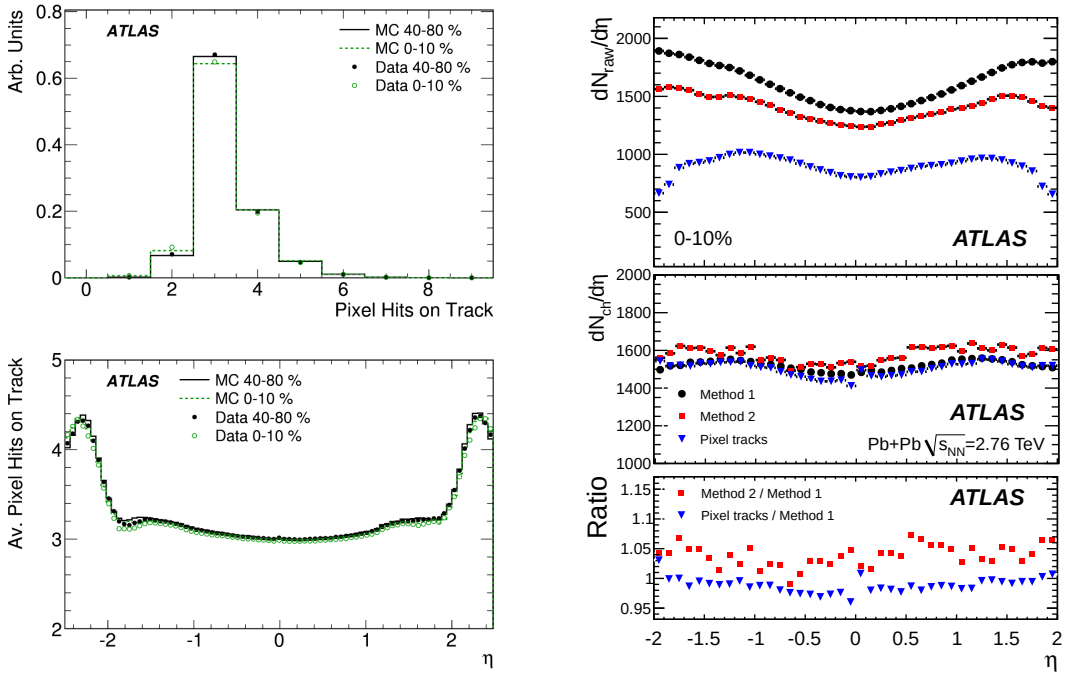

Figure 3: Pixel detector performance in Pb-Pb collisions: pixel points on tracks for central (0–10%) and peripheral (40–80%) events [7] (top-left), average number of pixel points as a function of track pseudorapidity (bottom-left). Measurement of the charged particle pseudorapidity distribution using three different pixel-only tracking algorithms (see text) [8]: raw track counting (top-right), after correction for acceptance and fake rate (middle-right) and relative comparison (bottom-right).

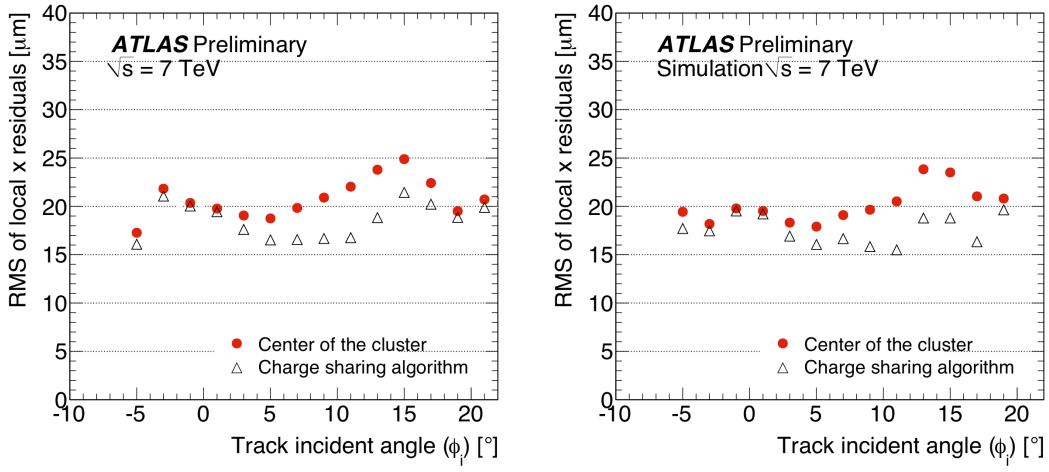

Figure 4: Residuals between track extrapolation and the measurement on the Pixel Detector, as a function of the track incident angle (corrected for the Lorentz angle, Sec. 5) for tracks with $p_{\mathrm{T}} > 5$ GeV. A pure digital readout (full circles) is compared with the *charge sharing* algorithm (open triangles) for data (left) and simulation (right).

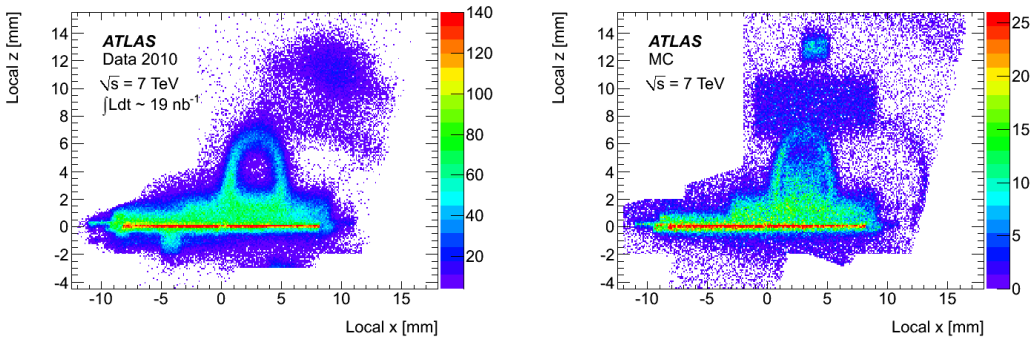

Figure 5: Distribution of reconstructed hadronic interaction in the Pixel Detector innermost layer for data (left panel) and the simplified description used in the simulation (right panel) [11].

6. Specific energy loss

The specific energy loss, $\mathrm{d}E/\mathrm{d}x$, associated to particles is measured from the charge collected in the pixel clusters, corrected for the length of path in silicon, after a selection that excludes regions where the charge collection efficiency is poor [12]. The track $\mathrm{d}E/\mathrm{d}x$ is defined as the truncated average of the energy deposition of each individual cluster, by removing the one with the highest normalized collected charge, in order to reduce the Landau tails. The distribution of the track $\mathrm{d}E/\mathrm{d}x$ is shown on the left panel of Fig. 7. A relative resolution of 11% is measured for particles with $p > 3$ GeV and at least three clusters per track. More details about the dependence of $\mathrm{d}E/\mathrm{d}x$ on the track momentum and charge are given in [5]. Separate bands for $\pi^{\pm}$, $K^{\pm}$ and $p(\bar{p})$ are identified. For positive charges also the band corresponding to deuterons is visible.

At first approximation, the specific energy loss depends only on the relativistic factor $\gamma\beta$ [13],

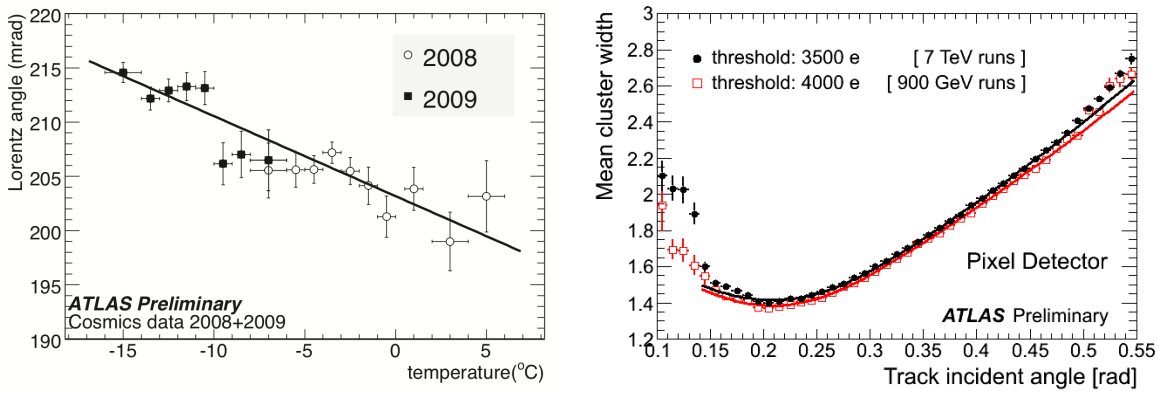

Figure 6: Lorentz angle measurements: temperature dependence measured on cosmic-ray data [3] (left) and average cluster size as a function of the track incident angle observed in 2009 $\sqrt{s} = 900$ GeV data and in 2010 $\sqrt{s} = 7$ TeV data (right).

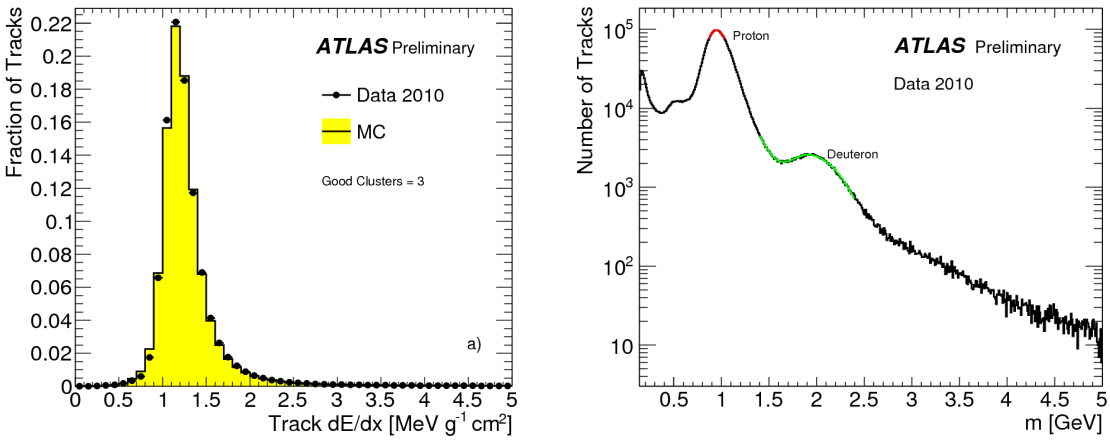

Figure 7: Left panel: distribution of the measured specific energy loss. Right panel: mass estimated inverting the Bethe-Bloch relation for a sample enhanced in heavy particles produced in hadronic interactions [12].

and its measurement can be combined with the particle momentum to give an estimation of the particle mass. The calibration can therefore be validated by reconstructing the mass peak of known particles. A sample enhanced in heavy particle content can be obtained by selecting tracks incompatible with the primary interaction vertex (impact parameter in the transvers plane 10 mm$<$ d_0 $<$100 mm) and high specific energy loss ($\mathrm{d}E/\mathrm{d}x > 1.9$ MeVg^{-1}cm^2). This sample contains a significant fraction of nuclei produced in hadronic interactions. The measured mass of these particles is shown in the right panel of Fig. 7, where the proton and deuteron peaks are clearly visible. This approach is used for the search of new long-lived heavy particles with the ATLAS detector [14].

7. Conclusions

The offline calibration procedure of the Pixel Detector includes a complete set of measurements which are performed in order to fully exploit its capability in the reconstruction and analysis of ATLAS events. The evolution of inefficiencies due to defective and noisy channels is monitored and fed into the detector simulation, resulting in an accurate estimation of tracking performance. High point resolution is provided by interpolating the signal shared among the pixels in cluster. The Lorentz angle and its temperature dependence are measured and used in the event reconstruction. The specific energy loss in the Pixel Detector modules is calibrated and used for the search of new particles predicted by extensions to the Standard Model.

References

[1] The ATLAS Collaboration, *The ATLAS Experiment at the CERN Large Hadron Collider*, *JINST* **3** (2008) S08003

[2] G. Aad et al., *ATLAS pixel detector electronics and sensors*, *JINST* **3** (2008) P07007

[3] The ATLAS Collaboration, *The ATLAS Inner Detector commissioning and calibration*, *Eur. Phys. J. C* **70** (2010) 787–821

[4] D. Hirschbül, *Operational experience of the ATLAS Pixel Detector*, contribution to these proceedings

[5] S. Martí-García, *Tracking and vertexing performance of the ATLAS Inner Detector at the LHC*, contribution to these proceedings

[6] A. Andreazza, *Test beam performance of the ATLAS Pixel Detector modules*, *Nucl. Instrum. Meth.* **A 565** (2006) 23–29

[7] The ATLAS Collaboration, *Measurement of the centrality dependence of J/ψ yields and observation of Z production in lead-lead collisions with the ATLAS detector at the LHC*, *Phys. Lett.* **B697** (2011) 294–312

[8] The ATLAS Collaboration, *Measurement of the centrality dependence of the charged particle pseudorapidity distribution in lead-lead collisions at $\sqrt{s_{NN}} = 2.76$ TeV with the ATLAS detector*, hep-ex 1108.6027

[9] S. Montesano, *Commissioning of the tracking system in the ATLAS detector*, Ph.D. Thesis, Università degli Studi di Milano, Milano, 2010, CERN-THESIS-2010-018

[10] I. Gorelov et al., *A measurement of Lorentz angle and spatial resolution of radiation hard silicon pixel sensors*, Nucl. Instrum. and Methods **A481** (2002), 204-221

[11] The ATLAS Collaboration, *A measurement of the material in the ATLAS Inner Detector using secondary hadronic interactions*, *JINST* **7** (2012) P01013

[12] The ATLAS Collaboration, *dE/dx measurement in the ATLAS Pixel Detector and its use for particle identification*, *ATLAS-CONF-2011-016*, CERN, Geneva

[13] K. Nakamura et al. (Particle Data Group), *The Review of Particle Physics*, *J. Phys.* **G 37** (2010), 075021

[14] The ATLAS Collaboration, *Search for Stable Hadronising Squarks and Gluinos at the ATLAS Experiment at the LHC*, *Phys. Lett.* **B 701** (2011) 1–19